CAKUT and Autonomic Dysfunction Caused by Acetylcholine Receptor Mutations

Nina Mann,[1,14] Franziska Kause,[1,14] Erik K. Henze,[2] Anant Gharpure,[3] Shirlee Shril,[1] Dervla M. Connaughton,[1] Makiko Nakayama,[1] Verena Klämbt,[1] Amar J. Majmundar,[1] Chen-Han W. Wu,[1] Caroline M. Kolvenbach,[1] Rufeng Dai,[1] Jing Chen,[1] Amelie T. van der Ven,[1] Hadas Ityel,[1] Madeleine J. Tooley,[4] Jameela A. Kari,[5] Lucy Bownass,[4] Sherif El Desoky,[5] Elisa De Franco,[6] Mohamed Shalaby,[5] Velibor Tasic,[7] Stuart B. Bauer,[8] Richard S. Lee,[8] Jonathan M. Beckel,[9] Weiqun Yu,[10] Shrikant M. Mane,[11] Richard P. Lifton,[11,12] Heiko Reutter,[13] Sian Ellard,[6] Ryan E. Hibbs,[3] Toshimitsu Kawate,[2] and Friedhelm Hildebrandt[1,*]

Congenital anomalies of the kidney and urinary tract (CAKUT) are the most common cause of chronic kidney disease in the first three decades of life, and *in utero* obstruction to urine flow is a frequent cause of secondary upper urinary tract malformations. Here, using whole-exome sequencing, we identified three different biallelic mutations in *CHRNA3*, which encodes the α3 subunit of the nicotinic acetylcholine receptor, in five affected individuals from three unrelated families with functional lower urinary tract obstruction and secondary CAKUT. Four individuals from two families have additional dysautonomic features, including impaired pupillary light reflexes. Functional studies *in vitro* demonstrated that the mutant nicotinic acetylcholine receptors were unable to generate current following stimulation with acetylcholine. Moreover, the truncating mutations p.Thr337Asnfs*81 and p.Ser340* led to impaired plasma membrane localization of CHRNA3. Although the importance of acetylcholine signaling in normal bladder function has been recognized, we demonstrate for the first time that mutations in *CHRNA3* can cause bladder dysfunction, urinary tract malformations, and dysautonomia. These data point to a pathophysiologic sequence by which monogenic mutations in genes that regulate bladder innervation may secondarily cause CAKUT.

Congenital anomalies of the kidney and urinary tract (CAKUT) represent up to 20%–30% of all prenatally detected anomalies and are the most common cause of chronic kidney disease in the first three decades of life.[1–3] The discovery of more than 40 monogenic causes of CAKUT in humans has led to the understanding that urogenital malformations often arise from defects in the signaling pathways that regulate nephrogenesis.[4–6] In addition, animal studies have demonstrated that intrauterine obstruction to urine flow can secondarily lead to CAKUT, although the genetic etiologies and molecular pathogenesis of these processes are not well understood.[7]

Nicotinic acetylcholine receptors (nAChR) are heteropentameric ligand-gated ion channels that are widely expressed in the nervous system and in certain non-neuronal tissues, such as the bladder urothelium.[8,9] Interestingly, mice lacking *Chrna3*, the gene encoding the α3 nAChR subunit, develop a prominent genitourinary phenotype, with reduced bladder contractility, megacystis, and recurrent urinary tract infections.[10] The α3 nAChR subunit mediates fast synaptic transmission in the parasympathetic, sympathetic, and enteric ganglia and plays a critical role in modulating normal bladder function.[11]

To date, only one gene involved in neuronal synaptic transmission, *CHRM3* (MIM: 118494), has been implicated in lower urinary tract obstruction in humans.[12] Here, we describe the discovery of biallelic mutations in *CHRNA3* in three families with CAKUT and additional extra-renal dysautonomic features.

Approval for human subject research was obtained from the Institutional Review Board at the respective institutions, and samples were obtained after written informed consent. The index case subject, B1717-21, is a young man who was born to consanguineous parents of Arabic descent and who presented in childhood with recurrent urinary tract infections. Renal ultrasound demonstrated bilateral hydronephrosis, a thickened bladder wall, and a large post-void residual (Figure 1A). Voiding cysturethrogram (VCUG) revealed bilateral grade 5 vesicoureteral reflux (VUR) without posterior urethral valves (not shown), and the affected individual was given a diagnosis of non-neurogenic neurogenic bladder. He developed progressive

[1]Department of Pediatrics, Boston Children's Hospital, Boston, MA 02115, USA; [2]Department of Molecular Medicine, Cornell University, Ithaca, NY 14853, USA; [3]Departments of Neuroscience and Biophysics, University of Texas Southwestern Medical Center, Dallas, TX 75390, USA; [4]Department of Clinical Genetics, St. Michael's Hospital, University Hospital's Bristol NHS Foundation Trust, Bristol BS2 8EG, UK; [5]Pediatric Nephrology Center of Excellence and Pediatric Department, Faculty of Medicine, King Abdulaziz University, Jeddah 21859, Kingdom of Saudi Arabia; [6]Institute of Biomedical and Clinical Science, University of Exeter Medical School, Exeter EX2 5DW, UK; [7]Medical Faculty Skopje, University Children's Hospital, Skopje 1000, Macedonia; [8]Department of Urology, Boston Children's Hospital, Boston, MA 02115, USA; [9]Department of Pharmacology and Chemical Biology, University of Pittsburgh, Pittsburgh, PA 15261, USA; [10]Division of Nephrology, Beth Israel Deaconess Medical Center, Boston, MA 02215, USA; [11]Department of Genetics, Yale University School of Medicine, New Haven, CT 06520, USA; [12]Laboratory of Human Genetics and Genomics, The Rockefeller University, New York, NY 10065, USA; [13]Institute of Human Genetics, University of Bonn, Bonn 53127, Germany Department of Neonatology and Pediatric Intensive Care, Children's Hospital, University of Bonn, Bonn 53127, Germany
[14]These authors contributed equally to this work
*Correspondence: friedhelm.hildebrandt@childrens.harvard.edu
https://doi.org/10.1016/j.ajhg.2019.10.004.

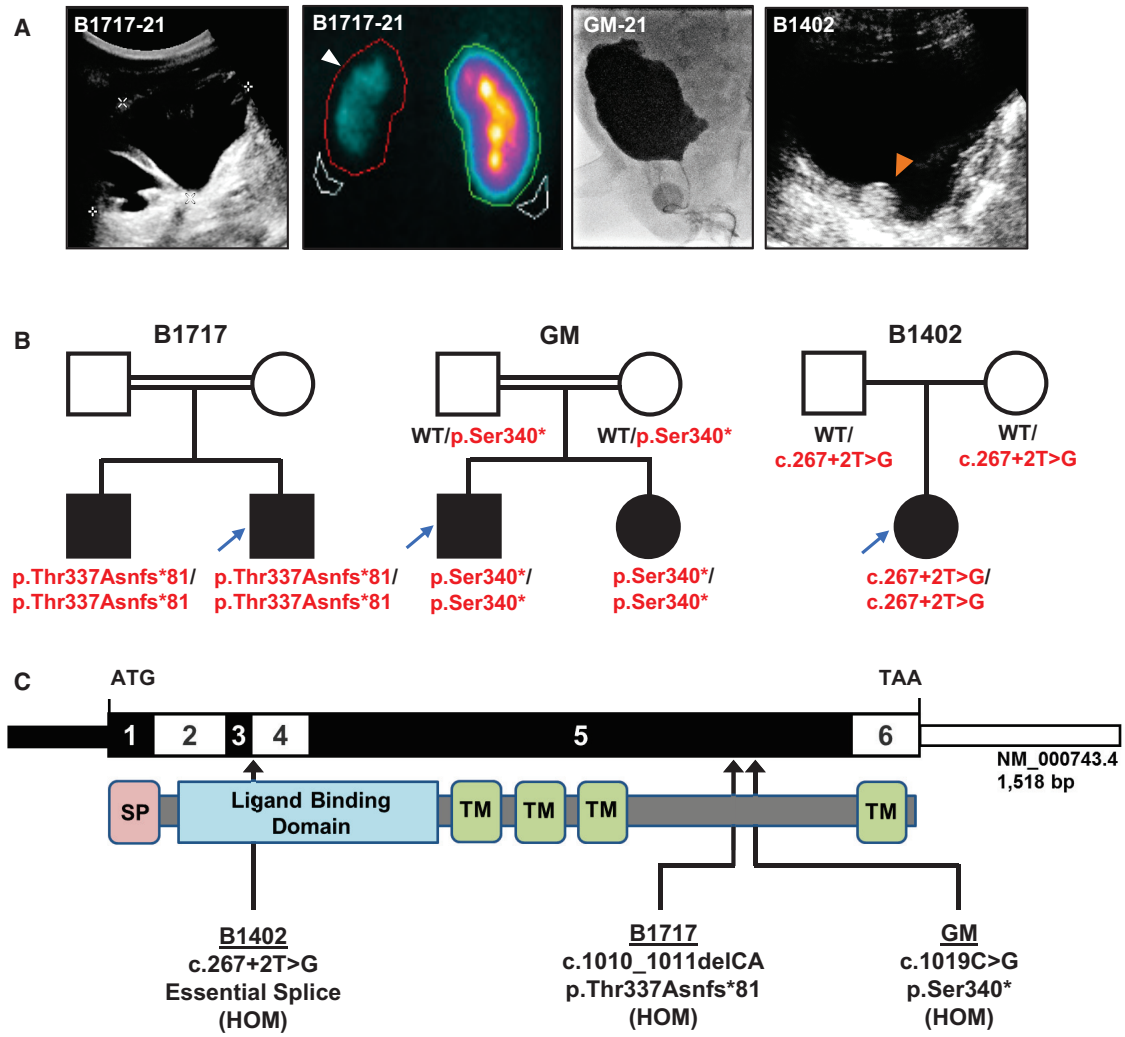

Figure 1. Identification of Biallelic *CHRNA3* Mutations in Three Families with CAKUT

(A) Renal and bladder imaging for affected individuals. The two left panels depict a renal ultrasound and DMSA (dimercaptosuccinic acid) scan from individual B1717-21. The renal ultrasound demonstrates severe left-sided hydronephrosis with cortical thinning, and DMSA scan shows reduced cortical uptake of the left kidney (arrow head). VCUG from individual GM-21 and bladder ultrasound from individual B1402 both demonstrate thickened and irregular bladder walls. The echogenic circular irregularity on the bladder ultrasound for B1402 (orange arrowhead) is an artifact from a STING procedure that was done after recurrent vesicoureteral reflux developed following bilateral ureteral reimplantation.

(B) Pedigrees for the three affected families. In the pedigrees, squares represent males and circles represent females. Open symbols represent unaffected individuals, and filled symbols represent affected individuals. Consanguineous unions are depicted as double horizontal lines. Probands (individuals -21 of each family) are denoted by blue arrows. WT, wild type.

(C) Exon and protein domain structure of *CHRNA3*. The exon structure is depicted in the upper bar, with positions of the start codon (ATG) and stop codon (TAA) indicated. The lower bar depicts the protein structure of CHRNA3, with an N-terminal signal peptide (pink), a large extracellular ligand-binding domain (blue), and four transmembrane helices (green). The three different mutations detected in three families are mapped to the exon and protein structures.

renal insufficiency, and by 19 years of age, a DMSA scan demonstrated a small, atrophic left kidney with 10% residual function (Figure 1A). He also presented to the ophthalmologist in adolescence for difficulty seeing in bright light and was found to have bilateral mydriasis with impaired pupillary constriction. Moreover, orthostatic hypotension was diagnosed on routine physical examination (Table 1). The proband's brother, B1717-22, was also noted to have an impaired pupillary light reflex. He additionally has a history of recurrent urinary tract infections, although renal ultrasound revealed normal-appearing kidneys and bladder (not shown).

We applied whole-exome sequencing (WES) and homozygosity mapping to individual B1717-21.[13,14] Mutation calling was performed in line with proposed guidelines by clinician-scientists who had knowledge of the clinical phenotypes and pedigree structure (Figure S1).[15] We identified a homozygous truncating mutation (GenBank: NM_000743.4; c.1010_1011delCA [p.Thr337Asnfs*81]) in exon 5 of the gene *CHRNA3* (Cholinergic Receptor

Table 1. Recessive Mutations Identified in *CHRNA3* in Three Families with CAKUT

Family	Ethnic Origin	Gender	Exon (Zygosity)	Nucleotide Change; Amino Acid Change (Segregation)[a]	gnomAD Allele Frequencies[b]	Genitourinary Manifestations	Dysautonomic Manifestations	Other[c]
B1402	Macedonian	female	intron 3 (hom)	c.267+2T>G (essential splice); (m. het; p. het)	0/1/246,220	bilat. VUR, grade IV recurrent VUR post ureteral reimplantation CKD (stage 2)	none	none
B1717-21	Arabic	male	exon 5 (hom)	c.1010_1011delCA (p.Thr337Asnfs*81); (ND)	NP	non-neurogenic neurogenic bladder bilat. VUR, grade V bilat. hydronephrosis atrophic left kidney CKD (stage 2)	impaired pupillary light reflex orthostatic hypotension	none
B1717-22	Arabic	male	exon 5 (hom)	c.1010_1011delCA (p.Thr337Asnfs*81); (ND)	NP	recurrent UTIs	impaired pupillary light reflex	none
GM-21	Pakistani	male	exon 5 (hom)	c.1019C>G (p.Ser340*); (m. het; p. het)	0/4/246,010	non-neurogenic neurogenic bladder left hydronephrosis right cystic kidney hypospadias	impaired pupillary light reflex flat CTG tracing *in utero*	hypertelorism broad nasal root intellectual disability 2q31.1-32.3 duplication (*de novo*)
GM-22	Pakistani	female	exon 5 (hom)	c.1019C>G (p.Ser340*); (m. het; p. het)	0/4/246,010	voiding dysfunction recurrent UTIs	impaired pupillary light reflex flat CTG tracing *in utero*	GERD, failure to thrive

Abbreviations: Bilat., bilateral; CKD, chronic kidney disease; CTG, cardiotocography; GERD, gastresophageal reflux; het, heterozygous; Hom, homozygous; m, maternal allele; ND, no data; NP, not present; p, paternal allele; UTI, urinary tract infection; VUR, vesicoureteral reflux.
[a]Segregation is listed as (maternal allele, paternal allele) when available. If parental DNA was not available, segregation is listed as ND.
[b]None of the identified *CHRNA3* mutations have been reported homozygously in gnomAD, which includes exome or genome sequencing data from 141,456 unrelated individuals.
[c]One affected individual was found to have additional genetic abnormalities that were thought to explain some of his extra-renal manifestations. GM-21 has a *de novo* 2q31.1–32.3 duplication which may explain his facial dysmorphisms and intellectual disability. This duplication was not shared by his sister, GM-22.

Nicotinic Alpha 3 Subunit), which encodes the α3 nAChR subunit. The same homozygous mutation was found in the proband's affected older brother, B1717-22 (Figure 1B, Table 1).

Through the use of the on-line tool, GeneMatcher,[16,17] we identified two siblings of Pakistani descent (GM-21 and GM-22) who also have biallelic mutations in *CHRNA3* (c.1019C>G [p.Ser340*]). GM-21 was diagnosed prenatally with hydronephrosis, and post-natal imaging revealed a dilated, cystic right kidney, left hydroureteronephrosis, and a thickened, trabeculated bladder wall (Figure 1A). He was diagnosed with non-neurogenic neurogenic bladder and was managed with clean intermittent catheterizations and subsequent vesicostomy. His younger sister, GM-22, had recurrent urinary tract infections, and VCUG demonstrated a large-capacity bladder with incomplete emptying (not shown). Ophthalmology examination for both children revealed constant miosis with pupils that did not dilate, and both siblings additionally had flat cardiotocography (CTG) tracings *in utero*. This was detected at 36 weeks gestational age in the older child, for which he underwent emergent cesarean section. A flat CTG tracing was noticed at 29 weeks gestational age for the younger sibling and persisted until she was delivered at full term.

We subsequently queried WES data in our cohort of 380 families with CAKUT and identified one additional affected individual with biallelic *CHRNA3* mutations. In individual B1402, who has bilateral VUR and hydronephrosis, we detected a homozygous essential splice site mutation (c.267+2T>G). Interestingly, this individual underwent ureteral reimplantation as a child but developed recurrence of her VUR, for which she underwent a STING procedure (Figure 1A). We did not detect any biallelic mutations in *CHRNA3* in a control cohort of 419 families with either nephrotic syndrome or nephronophthisis.

All three *CHRNA3* mutations were confirmed via Sanger sequencing (Figure S3). A summary of the clinical characteristics of the affected individuals and the mutations identified is provided in Table 1, and a schematic of the *CHRNA3* exon and protein structure with locations of the three mutations is depicted in Figure 1C. Both the p.Thr337Asnfs*81 and p.Ser340* variants are predicted to lead to premature termination of the protein prior to the fourth transmembrane helix (Figure 1C). As RNA was not available from the individual with the c.267+2T>G splice mutation, we used *in silico* prediction tools to determine the splicing effect. Because the c.267+2T>G change occurs at an obligatory splice site, we predict that this will lead to skipping of exon 3 and an in-frame deletion of 15 amino acids in the protein's extracellular ligand-binding domain. However, it should be noted that this may not recapitulate the splicing effect *in vivo*.

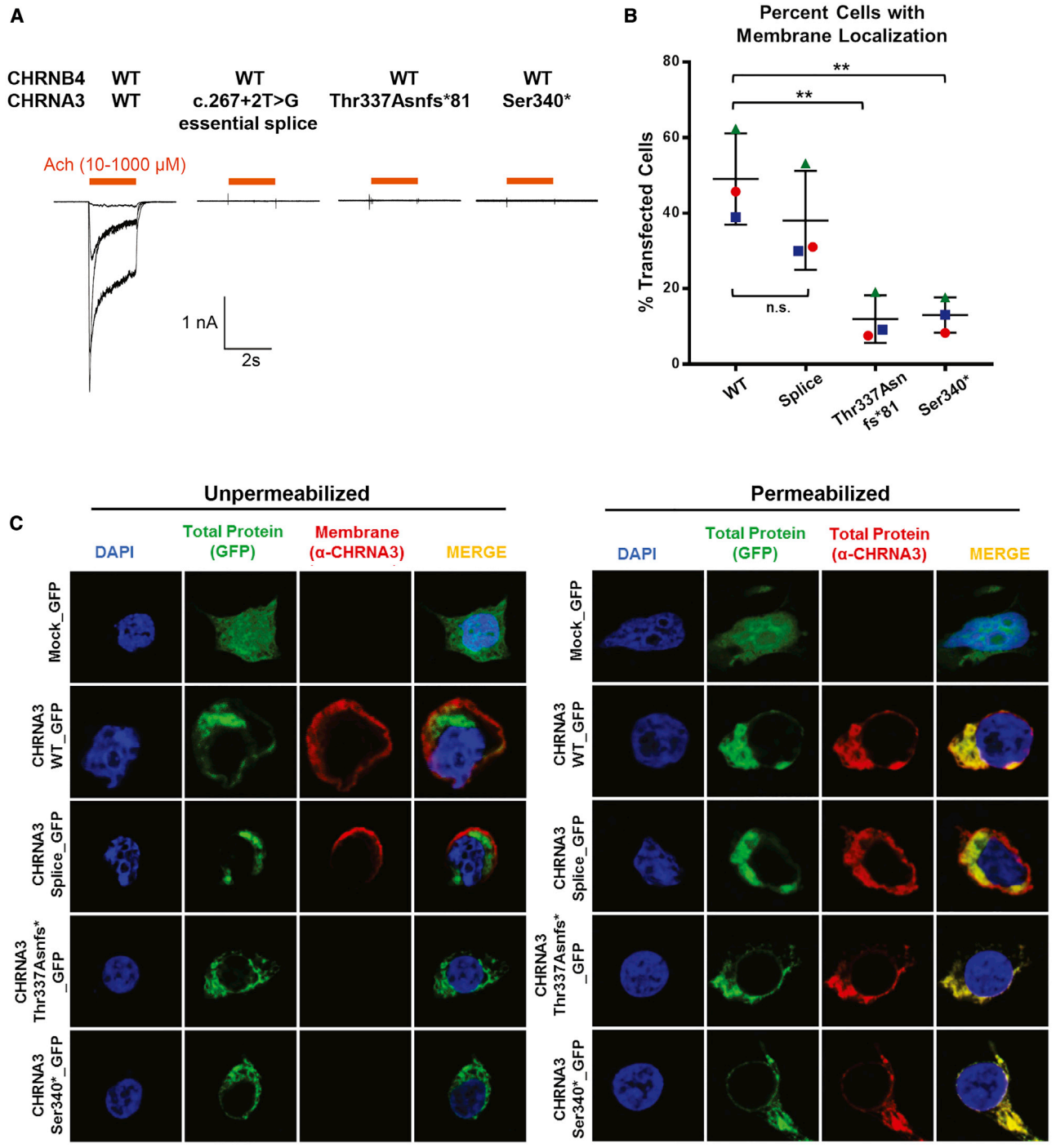

Figure 2. *CHRNA3* Mutants Perturb α3β4 nAChR Function and Impair Plasma Membrane Trafficking

(A) Whole-cell currents obtained from HEK293 cells overexpressing both wild-type and the indicated mutant α3β4 nicotinic acetylcholine receptors (nAChRs). Wild-type α3β4 nAChR generates a strong current after incubation with acetylcholine (n = 7). In contrast, the essential splice (n = 4), p.Thr337Asnfs*81 (n = 4), and p.Ser340* (n = 4) mutants were unable to generate any current.

(B) Membrane localization of α3 nAChR in HEK293 cells. Quantification of immunofluorescence images of HEK293 cells overexpressing either wild-type or mutant GFP-tagged CHRNA3. Graphs represent an average of three independent experiments. For each experiment, 100–150 transfected cells were evaluated for membrane staining. 49% of cells transfected with WT-CHRNA3 demonstrated membrane staining. In contrast, only 12%–13% of cells transfected with the p.Thr337Asnfs*81 and p.Ser340* mutants demonstrate membrane staining, respectively. The error bars represent SEM for three experiments. **p value < 0.01 when compared to wild type; n.s. not significant when compared to wild type.

(C) Representative immunofluorescence images depicting the cellular localization of overexpressed GFP-tagged wild-type and mutant α3 nAChRs in HEK293 cells. Unpermeabilized (left) and permeabilized (right) cells are stained with an anti-CHRNA3 antibody raised against the protein's extracellular N terminus. The green GFP signal demonstrates total transfected CHRNA3 protein, whereas in

(legend continued on next page)

In the two families in which homozygosity mapping was available, the *CHRNA3* mutations were all located within regions of homozygosity by descent (Figure S4). None of the three *CHRNA3* variants were present homozygously in the large population database, gnomAD (Table 1). Exome data for each proband from the three families were also analyzed for mutations in known CAKUT genes[5] and no causative variants were identified. However, individual GM-21 was noted to have a *de novo* 25.6 Mb duplication of chromosome 2q31.1–2q32.3 that was not shared by his affected sister. This is thought to contribute to his cognitive deficits, although further studies will be required for causality to be more definitively established.

In order to examine whether the identified mutations in *CHRNA3* affect receptor function, we performed electrophysiology and immunofluorescence studies in HEK293 cells. The α3 nAChR subunit is known to heteropentamerize with the β4 nAChR subunit,[18] and we first aimed to determine whether the *CHRNA3* mutations affect the ability of the α3β4 nAChR to induce current after stimulation with acetylcholine. Patch-clamping experiments were performed in HEK293 cells co-transfected with wild-type *CHRNB4* cDNA and either wild-type or mutant *CHRNA3* cDNA. Acetylcholine induced a dose-dependent inward current in cells overexpressing the wild-type α3β4 nAChR (Figure 2A). In contrast, no current was generated in cells expressing receptors composed of the splice site, p.Thr337Asnfs81*, or p.Ser340* mutant α3 subunits (Figure 2A). These data demonstrate complete loss of function for the essential splice and two truncating variants.

Because the two truncating mutations (p.Thr337Asnfs*81 and p.Ser340*) lead to premature termination of the CHRNA3 protein prior to the fourth transmembrane helix, we hypothesized that this would disrupt membrane trafficking of the mutant receptors. We expressed GFP-tagged wild-type and mutant *CHRNA3* cDNA in HEK293 cells and labeled unpermeabilized cells with an antibody to the extracellular N terminus of the α3 nAChR subunit, which is expected to bind only those proteins that are inserted into the plasma membrane (Figures 2B and 2C). We detected membrane localization of the wild-type α3 nAChR subunit in 49% of transfected cells. In contrast, only 12%–13% of transfected cells demonstrated membrane staining for the p.Thr337Asnfs*81 and p.Ser340* mutants, suggesting impaired membrane trafficking (Figure 2B). There is a trend toward reduced membrane localization for the essential splice site variant, but this did not reach statistical significance. Representative immunofluorescence images are depicted in Figure 2C. Permeabilized cells, in which both extracellular and intracellular labeling is established, were utilized as controls.

We here discovered by whole-exome sequencing three different homozygous loss-of-function mutations in *CHRNA3* in three families with CAKUT. We demonstrate that all three mutations attenuate the ability of the α3β4 nAChR to generate current after stimulation with acetylcholine. Additionally, the two truncating mutations, p.Thr337Asnfs* and p.Ser340*, impair receptor trafficking to the plasma membrane.

Micturition requires coordinated stimulation of the urinary bladder and urethral sphincters by the parasympathetic, sympathetic, and somatic nervous systems (Figure S5).[11] *CHRNA3* mediates fast synaptic transmission in the autonomic ganglia, and we predict that loss of *CHRNA3* may result in discoordinated detrusor and urethral function. *CHRNA3* is also expressed in the bladder urothelium and therefore may play additional roles in regulating bladder contraction beyond its known function in the autonomic ganglia.[9] Of interest, all three families in our cohort developed secondary upper urinary tract malformations, such as hydronephrosis and renal cysts, consistent with the notion that obstruction to urinary flow *in utero* can lead to abnormalities in renal development.[7,19,20] Indeed, individual B1402 underwent bilateral ureteral reimplantation, only to develop recurrent VUR and worsening hydronephrosis, likely because her underlying bladder dysfunction had not been recognized. We propose that disruption of *CHRNA3* can result in a pathophysiological sequence by which impaired neuronal innervation leads to bladder dysfunction, functional lower urinary tract obstruction, and subsequent upper urinary tract anomalies.

In addition to their renal manifestations, families B1717 and GM, in whom truncating *CHRNA3* mutations were found, have dysautonomic features, most notably an impaired pupillary light reflex. Compellingly, autoantibodies to the α3 nAChR subunit have been described to cause an autoimmune autonomic ganglionopathy in humans.[21] These individuals develop profound autonomic failure, with symptoms overlapping those found in families with truncating *CHRNA3* mutations, including bladder dysfunction, impaired pupillary light reflexes, and orthostatic hypotension.[21,22] Notably, individual B1402 does not have dysautonomic manifestations. This may be due to subtle findings that are not clinically manifest, or it may be the case that hypomorphic mutations lead to a milder phenotype. Identification of additional affected individuals with *CHRNA3* mutations may provide further insight into genotype-phenotype correlations.

unpermeabilized cells, the red signal (anti-CHRNA3) depicts protein localized to the plasma membrane. Wild-type CHRNA3 and the splice site mutant both demonstrate membrane localization. In contrast, there is no signal from the anti-CHRNA3 antibody for the protein truncating p.Thr337Asnfs* and p.Ser340* mutants, suggesting impaired membrane localization. In permeabilized cells, both the GFP signal (green) and antibody staining (red) demonstrate cytoplasmic localization of the p.Thr337Asnfs* and p.Ser340* mutant proteins.

The genitourinary and ocular phenotypes seen in families B1717 and GM are strikingly similar to that of the *Chrna3*$^{-/-}$ mice, which have megacystis, recurrent urinary tract infections, and persistent mydriasis.[10] Bladder strips from these animals fail to contract in response to nicotine, and neurons from the superior cervical ganglia do not generate current in response to acetylcholine, consistent with the notion that loss of *CHRNA3* results in impaired fast synaptic transmission within the autonomic ganglia.[10] It is interesting to note that there is variable expressivity among affected individuals with *CHRNA3* mutations. The two siblings in family B1717, who harbor the same *CHRNA3* p.Thr337Asnfs*87 truncating mutation, for example, exhibit a range of renal phenotypes, from only recurrent urinary tract infections to severe hydronephrosis, vesicoureteral reflux, and chronic kidney disease. This supports the notion that the renal disease manifesting in these individuals is the result of a pathophysiological sequence whereby impairment of bladder contraction results in secondary upper urinary tract malformations. The degree of renal impairment is likely a result of stochastic changes that occur *in utero*, and such variable expressivity is often seen in a variety of other monogenic diseases that cause CAKUT.[4,23]

To date, few monogenic causes of bladder dysfunction have been described in humans, including mutations in the genes *CHRM3* (MIM: 118494), *ACTG2* (MIM: 102545), *ACTA2* (MIM: 102620), *MYH11* (MIM: 160745), *MYLK* (MIM: 600922), *HPSE2* (MIM: 613469), and *LRIG2* (MIM: 608869).[12,24–30] These genes have been implicated in the regulation of smooth muscle actin contraction, neuronal patterning, and synaptic neuronal transmission (Figure S5), and mutations cause syndromes such as megacystis-microcolon-intestinal hypoperistalsis syndrome (MMIHS [MIM: 155310, 613834]) or urofacial syndrome (MIM: 236730, 615112). Interestingly, individuals with mutations in *CHRM3*, which encodes a muscarinic acetylcholine receptor, also present with persistent mydriasis.[12] The findings in our study provide additional evidence that disruption of the neural pathways regulating bladder function can be important genetic causes of both CAKUT and autonomic dysfunction in humans.

Our findings may point to important therapeutic implications. Current management for children with lower urinary obstruction involves surgical intervention to relieve anatomic obstruction and subsequent medical management of the sequelae from chronic kidney disease.[31] However, surgical techniques alone may not be successful for individuals in whom mutations in *CHRNA3* are identified, as was the case for individual B1402. The neuronal pathways regulating bladder contraction additionally provide tractable therapeutic targets that may be amenable to pharmacological intervention. In addition, early prenatal genetic diagnoses might eventually allow for pharmacological interventions *in utero*, which could prevent the development of renal dysgenesis. Further identification of novel genetic causes of urinary tract obstruction will provide additional strategies toward precision medicine.

Supplemental Data

Supplemental Data can be found online at https://doi.org/10.1016/j.ajhg.2019.10.004.

Acknowledgments

We thank the affected individuals and their families for their contributions to this study. We also would like to thank Michael Wangler, Arthur Beaudet, Reza Bekheirnia, William Newman, and Fowzan Alkuraya for helpful discussion. This research was supported by grants from the National Institutes of Health to F.H. (DK0668306). N.M. is supported by funding from the National Institutes of Health (grant T32-DK007726). F.K. is supported by funding from the Biomedical Education Program. D.M.C. is funded by the Health Research Board, Ireland (HPF-206-674), the International Pediatric Research Foundation Early Investigators' Exchange Program, and the Amgen Irish Nephrology Society Specialist Registrar Bursary. M.N. is supported by a grant from the Japan Society for the Promotion of Science. V.K. is supported by the Deutsche Forschungsgemeinschaft (403877094). A.J.M. is supported by funding from the National Institutes of Health (grant T32-DK007726), the 2017 Harvard Stem Cell Institute Fellowship Grant, and the 2018 Jared J. Grantham Research Fellowship from the American Society of Nephrology Ben J. Lipps Research Fellowship Program. C.-H.W.W. is supported by funding from the National Institutes of Health (grant T32-GM007748). R.S.L. is supported by funding from the National Institutes of Health (DK096238). S.E. is a Wellcome Senior Investigator. F.H. is also supported by the Begg Family Foundation. We also thank the Yale Center for Mendelian Genomics for whole-exome sequencing analysis (U54HG006504).

Declaration of Interests

F.H. is a cofounder and S.A.C. member and holds stocks in Goldfinch-Bio. All other authors declare that they have no competing financial interests.

Received: June 11, 2019
Accepted: October 9, 2019
Published: November 7, 2019

Web Resources

1000 Genomes Project, https://www.internationalgenome.org/1000-genomes-browsers
Clustal Omega, https://www.ebi.ac.uk/Tools/msa/clustalo/
Exome Aggregation Consortium (ExAC), http://exac.broadinstitute.org
GenBank, https://www.ncbi.nlm.nih.gov/genbank/
Genome Aggregation Database (gnomAD), http://gnomad.broadinstitute.org
MutationTaster, http://www.mutationtaster.org
NHLBI Exome Sequencing Project (ESP), https://evs.gs.washington.edu/EVS
Online Mendelian Inheritance in Man (OMIM), https://www.omim.org
PolyPhen2, http://genetics.bwh.harvard.edu/pph2

Sorting Intolerant From Tolerant (SIFT), http://sift.jcvi.org
UCSC Genome Browser, https://genome.ucsc.edu

References

1. Ingelfinger, J.R., Kalantar-Zadeh, K., Schaefer, F.; and World Kidney Day Steering Committee (2016). World Kidney Day 2016: Averting the legacy of kidney disease-focus on childhood. Pediatr. Nephrol. *31*, 343–348.
2. Calderon-Margalit, R., Golan, E., Twig, G., Leiba, A., Tzur, D., Afek, A., Skorecki, K., and Vivante, A. (2018). History of Childhood Kidney Disease and Risk of Adult End-Stage Renal Disease. N. Engl. J. Med. *378*, 428–438.
3. Queisser-Luft, A., Stolz, G., Wiesel, A., Schlaefer, K., and Spranger, J. (2002). Malformations in newborn: results based on 30,940 infants and fetuses from the Mainz congenital birth defect monitoring system (1990-1998). Arch. Gynecol. Obstet. *266*, 163–167.
4. van der Ven, A.T., Vivante, A., and Hildebrandt, F. (2018). Novel Insights into the Pathogenesis of Monogenic Congenital Anomalies of the Kidney and Urinary Tract. J. Am. Soc. Nephrol. *29*, 36–50.
5. van der Ven, A.T., Connaughton, D.M., Ityel, H., Mann, N., Nakayama, M., Chen, J., Vivante, A., Hwang, D.Y., Schulz, J., Braun, D.A., et al. (2018). Whole-Exome Sequencing Identifies Causative Mutations in Families with Congenital Anomalies of the Kidney and Urinary Tract. J. Am. Soc. Nephrol. *29*, 2348–2361.
6. Verbitsky, M., Westland, R., Perez, A., Kiryluk, K., Liu, Q., Krithivasan, P., Mitrotti, A., Fasel, D.A., Batourina, E., Sampson, M.G., et al. (2019). The copy number variation landscape of congenital anomalies of the kidney and urinary tract. Nat. Genet. *51*, 117–127.
7. Chevalier, R.L., Thornhill, B.A., Forbes, M.S., and Kiley, S.C. (2010). Mechanisms of renal injury and progression of renal disease in congenital obstructive nephropathy. Pediatr. Nephrol. *25*, 687–697.
8. Albuquerque, E.X., Pereira, E.F., Alkondon, M., and Rogers, S.W. (2009). Mammalian nicotinic acetylcholine receptors: from structure to function. Physiol. Rev. *89*, 73–120.
9. Beckel, J.M., Kanai, A., Lee, S.J., de Groat, W.C., and Birder, L.A. (2006). Expression of functional nicotinic acetylcholine receptors in rat urinary bladder epithelial cells. Am. J. Physiol. Renal Physiol. *290*, F103–F110.
10. Xu, W., Gelber, S., Orr-Urtreger, A., Armstrong, D., Lewis, R.A., Ou, C.N., Patrick, J., Role, L., De Biasi, M., and Beaudet, A.L. (1999). Megacystis, mydriasis, and ion channel defect in mice lacking the alpha3 neuronal nicotinic acetylcholine receptor. Proc. Natl. Acad. Sci. USA *96*, 5746–5751.
11. Fowler, C.J., Griffiths, D., and de Groat, W.C. (2008). The neural control of micturition. Nat. Rev. Neurosci. *9*, 453–466.
12. Weber, S., Thiele, H., Mir, S., Toliat, M.R., Sozeri, B., Reutter, H., Draaken, M., Ludwig, M., Altmüller, J., Frommolt, P., et al. (2011). Muscarinic Acetylcholine Receptor M3 Mutation Causes Urinary Bladder Disease and a Prune-Belly-like Syndrome. Am. J. Hum. Genet. *89*, 668–674.
13. Braun, D.A., Lovric, S., Schapiro, D., Schneider, R., Marquez, J., Asif, M., Hussain, M.S., Daga, A., Widmeier, E., Rao, J., et al. (2018). Mutations in multiple components of the nuclear pore complex cause nephrotic syndrome. J. Clin. Invest. *128*, 4313–4328.
14. Hildebrandt, F., Heeringa, S.F., Rüschendorf, F., Attanasio, M., Nürnberg, G., Becker, C., Seelow, D., Huebner, N., Chernin, G., Vlangos, C.N., et al. (2009). A systematic approach to mapping recessive disease genes in individuals from outbred populations. PLoS Genet. *5*, e1000353.
15. MacArthur, D.G., Manolio, T.A., Dimmock, D.P., Rehm, H.L., Shendure, J., Abecasis, G.R., Adams, D.R., Altman, R.B., Antonarakis, S.E., Ashley, E.A., et al. (2014). Guidelines for investigating causality of sequence variants in human disease. Nature *508*, 469–476.
16. Sobreira, N., Schiettecatte, F., Boehm, C., Valle, D., and Hamosh, A. (2015). New tools for Mendelian disease gene identification: PhenoDB variant analysis module; and GeneMatcher, a web-based tool for linking investigators with an interest in the same gene. Hum. Mutat. *36*, 425–431.
17. Sobreira, N., Schiettecatte, F., Valle, D., and Hamosh, A. (2015). GeneMatcher: a matching tool for connecting investigators with an interest in the same gene. Hum. Mutat. *36*, 928–930.
18. Skok, V.I. (2002). Nicotinic acetylcholine receptors in autonomic ganglia. Auton. Neurosci. *97*, 1–11.
19. Chevalier, R.L., Forbes, M.S., and Thornhill, B.A. (2009). Ureteral obstruction as a model of renal interstitial fibrosis and obstructive nephropathy. Kidney Int. *75*, 1145–1152.
20. Becknell, B., Carpenter, A.R., Allen, J.L., Wilhide, M.E., Ingraham, S.E., Hains, D.S., and McHugh, K.M. (2013). Molecular basis of renal adaptation in a murine model of congenital obstructive nephropathy. PLoS ONE *8*, e72762.
21. Vernino, S., Sandroni, P., Singer, W., and Low, P.A. (2008). Invited Article: Autonomic ganglia: target and novel therapeutic tool. Neurology *70*, 1926–1932.
22. Vernino, S., Low, P.A., Fealey, R.D., Stewart, J.D., Farrugia, G., and Lennon, V.A. (2000). Autoantibodies to ganglionic acetylcholine receptors in autoimmune autonomic neuropathies. N. Engl. J. Med. *343*, 847–855.
23. Vivante, A., and Hildebrandt, F. (2016). Exploring the genetic basis of early-onset chronic kidney disease. Nat. Rev. Nephrol. *12*, 133–146.
24. Wangler, M.F., Gonzaga-Jauregui, C., Gambin, T., Penney, S., Moss, T., Chopra, A., Probst, F.J., Xia, F., Yang, Y., Werlin, S., et al.; Baylor-Hopkins Center for Mendelian Genomics (2014). Heterozygous de novo and inherited mutations in the smooth muscle actin (ACTG2) gene underlie megacystis-microcolon-intestinal hypoperistalsis syndrome. PLoS Genet. *10*, e1004258.
25. Milewicz, D.M., Østergaard, J.R., Ala-Kokko, L.M., Khan, N., Grange, D.K., Mendoza-Londono, R., Bradley, T.J., Olney, A.H., Adès, L., Maher, J.F., et al. (2010). De novo ACTA2 mutation causes a novel syndrome of multisystemic smooth muscle dysfunction. Am. J. Med. Genet. A. *152A*, 2437–2443.
26. Daly, S.B., Urquhart, J.E., Hilton, E., McKenzie, E.A., Kammerer, R.A., Lewis, M., Kerr, B., Stuart, H., Donnai, D., Long, D.A., et al. (2010). Mutations in HPSE2 cause urofacial syndrome. Am. J. Hum. Genet. *86*, 963–969.
27. Stuart, H.M., Roberts, N.A., Burgu, B., Daly, S.B., Urquhart, J.E., Bhaskar, S., Dickerson, J.E., Mermerkaya, M., Silay, M.S., Lewis, M.A., et al. (2013). LRIG2 mutations cause urofacial syndrome. Am. J. Hum. Genet. *92*, 259–264.
28. Roberts, N.A., Hilton, E.N., Lopes, F.M., Singh, S., Randles, M.J., Gardiner, N.J., Chopra, K., Coletta, R., Bajwa, Z., Hall,

R.J., et al. (2019). Lrig2 and Hpse2, mutated in urofacial syndrome, pattern nerves in the urinary bladder. Kidney Int. *95*, 1138–1152.

29. Halim, D., Brosens, E., Muller, F., Wangler, M.F., Beaudet, A.L., Lupski, J.R., Akdemir, Z.H.C., Doukas, M., Stoop, H.J., de Graaf, B.M., et al. (2017). Loss-of-Function Variants in MYLK Cause Recessive Megacystis Microcolon Intestinal Hypoperistalsis Syndrome. Am. J. Hum. Genet. *101*, 123–129.
30. Gauthier, J., Ouled Amar Bencheikh, B., Hamdan, F.F., Harrison, S.M., Baker, L.A., Couture, F., Thiffault, I., Ouazzani, R., Samuels, M.E., Mitchell, G.A., et al. (2015). A homozygous loss-of-function variant in MYH11 in a case with megacystis-microcolon-intestinal hypoperistalsis syndrome. Eur. J. Hum. Genet. *23*, 1266–1268.
31. Chevalier, R.L. (2015). Congenital urinary tract obstruction: the long view. Adv. Chronic Kidney Dis. *22*, 312–319.

The American Journal of Human Genetics, Volume *105*

Supplemental Data

CAKUT and Autonomic Dysfunction Caused by Acetylcholine Receptor Mutations

Nina Mann, Franziska Kause, Erik K. Henze, Anant Gharpure, Shirlee Shril, Dervla M. Connaughton, Makiko Nakayama, Verena Klämbt, Amar J. Majmundar, Chen-Han W. Wu, Caroline M. Kolvenbach, Rufeng Dai, Jing Chen, Amelie T. van der Ven, Hadas Ityel, Madeleine J. Tooley, Jameela A. Kari, Lucy Bownass, Sherif El Desoky, Elisa De Franco, Mohamed Shalaby, Velibor Tasic, Stuart B. Bauer, Richard S. Lee, Jonathan M. Beckel, Weiqun Yu, Shrikant M. Mane, Richard P. Lifton, Heiko Reutter, Sian Ellard, Ryan E. Hibbs, Toshimitsu Kawate, and Friedhelm Hildebrandt

Supplemental Appendix

SUPPLEMENTAL METHODS

Whole exome sequencing and homozygosity mapping. We obtained blood samples and pedigree information following informed consent from individuals with CAKUT. Approval for human subjects research was obtained from the Institutional Review Board at the respective institutions. Whole exome sequencing was performed as described previously using Agilent SureSelect™ human exome capture arrays (ThermoFisher) with next generation sequencing (NGS) on an Illumina™ platform (1). Sequence reads were mapped against the human reference genome (NCBI build 37/hg19) using CLC Genomics Workbench (version 6.5.1) (CLC bio). For homozygosity mapping, downstream processing of aligned BAM files were performed using Picard and samtools. SNV calling was done using GATK5 and the generated VCF file was subsequently used in homozygosity mapper. Genetic regions of homozygosity by descent were plotted across the genome as candidate regions for recessive genes as previously described (2). Mutation calling was performed in line with proposed guidelines by clinician-scientists who had knowledge of clinical phenotypes, pedigree structure, and genetic mapping (**Supplemental Figure 1**) (3). All variants were confirmed in original DNA using Sanger sequencing. The website GeneMatcher (https://genematcher.org/statistics) enabled the connection between researchers and providers caring for the families (4, 5).

cDNA cloning. Full length human *CHRNA3* (NM_000734.4) and *CHRNB4* (NM_000750.5) cDNAs were purchased from the Harvard PlasmID database (https://plasmid.med.harvard.edu). Human *CHRNA3* and *CHRNB4* (NM_000750.5) full-length cDNA and the two truncating variants, c.1010_1011delCA and c.1019C>G, were subcloned by PCR into the pENTR-D-TOPO vector (Thermo Fisher Scientific). Mutagenesis was performed using the QuikChange II XL site-directed mutagenesis kit (Agilent Technologies) to generate the c.267+2T>G and c.1010_1011delCA mutants. To represent the essential splice site mutation, c.267+2T>G, which is predicted to lead to in-frame skipping of exon 3, we generated a cDNA construct with exon 3 deleted. Primers used for subcloning and mutagenesis are listed in **Supplementary Table S1**. Expression vectors were generated using LR clonase (Thermo Fisher Scientific) following the manufacturer's instruction. The expression vector pcDNA6.2-C-GFP (Thermo Fisher Scientific) was used in this publication.

Cell culture and transient transfections. Experiments were performed in HEK293 cells purchased from the American Type Culture Collection (ATCC) biological resource center. For transient transfections, HEK293 cells were seeded at 40-50% confluency in DMEM, supplemented with 10% fetal calf serum and 1% penicillin/streptomycin and grown overnight. Transfections were carried out using Lipofectamine2000 (Thermo Fisher Scientific) and OptiMEM (Thermo Fisher Scientific) following the manufacturer's instructions. Cell lines were tested monthly for mycoplasma contamination.

Immunofluorescence and confocal microscopy in cell lines. For immunostaining, HEK293 cells were seeded on Fibronectin-coated coverslips in 6-well plates. After 24 hours, cells were transiently transfected with 800-1000ng of DNA using Lipofectamine2000 (Thermo Fisher Scientific) following the manufacturer's instructions. Experiments were performed 24–48 hours after transfection. Cells were fixed for 10 minutes using 2% paraformaldehyde at room temperature. If permeabilization was done, cells were incubated for 10 minutes in 0.5% Triton X-100. For immunostaining of unpermeabilized cells, this permeabilization step was skipped. Cells were then blocked with 10% donkey serum + 1% BSA and incubated with primary antibody overnight at 4°C. The following day, cells were incubated in secondary antibody for 60 minutes at room temperature, and subsequently stained for 5 minutes with 4',6-diamidino-2-phenylindole (DAPI) in PBS. Confocal imaging was performed using the Leica SP5X system with an upright DM6000 microscope, and images were processed with the Leica AF software suite. Immunofluorescence experiments were repeated at least three times in independent experiments. The following antibodies were used for immunofluorescence experiments with similar results: rabbit anti-CHRNA3 (SAB2104205, Sigma), diluted 1:100 and rabbit anti-CHRNA3 (NBP2-30060, Novus), diluted 1:100. Donkey anti-rabbit secondary antibody conjugated to Alexa Fluor 594 was purchased from Invitrogen.

Whole cell electrophysiology in HEK293 cells. All chemicals were purchased from Sigma-Aldrich unless otherwise noted. HEK293 cells used for electrophysiology experiments were purchased from ATCC and were used from passages 5-30. Cells were maintained in DMEM (Gibco) supplemented with 10% FBS (Atlanta Biologicals) and 10 ug/ml gentamicin (Gibco). Two days prior to recording, HEK293 cells were plated at low density onto 12 mm glass coverslips (VWR) in wells of a 6-well plate (Greiner). Cells were transfected with 300-700 ng DNA after 24 hours using FuGENE6 (Promega) according to the manufacturer's instructions. Whole cell electrophysiological recordings were carried out 16-24 hours after transfection. Borosilicate glass pipettes (Harvard Apparatus) were pulled and heat polished to a final resistance of 2-4 MΩ and backfilled with (in mM) 147 NaCl, 10 EGTA, and 10 HEPES (adjusted to pH 7.0 with NaOH). Patches were obtained in an external buffer containing (in mM) 147 NaCl, 2 KCl, 2 $CaCl_2$, 1 $MgCl_2$, 13 glucose, 10 HEPES (adjusted to pH 7.3 with NaOH), then perfused with acetylcholine (ACh) using a rapid solution exchange system (RSC-200; Bio-Logic). Currents were recorded using an Axopatch 200B patch clamp amplifier (Axon Instruments), filtered at 2 kHz (Frequency Devices), digitized with a Digidata 1440A (Axon Instruments) with a sampling frequency of 10 kHz, and analyzed using the pCLAMP 10.5 software (Axon Instruments).

Table S1: Primer sequences used for subcloning and mutagenesis.

Human *CHRNA3* pENTR cloning primer sequences		
Target	Forward Primer (5'-3')*	Reverse Primer (5'-3')
Wild Type	CACCATGGGCTCTGGCCCGCTC	TGCATCTTCCCTGGCC
Thr337Asnfs*81	CACCATGGGCTCTGGCCCGCTC	GCACTGAAATTGGAGATTTTTATCC
Ser340*	CACCATGGGCTCTGGCCCGCTC	GGGCATTGTGTGTGTCGTC
Human *CHRNA3* mutagenesis primer sequences		
Target	Forward Primer (5'-3')	Reverse Primer (5'-3')
Essential Splice (Exon 3 skipping)	TCTCAGCTGGTGAAGGTGATCTGGAATG ACTACAAG	CTTGTAGTCATTCCAGATCACCTTCACCA GCTGAGA
Thr337Asnfs*81	CCCGACGACACACAATGCCCTCATGGGT	ACCCATGAGGGCATTGTGTGTCGTCGGG
Human *CHRNB4* pENTR cloning primer sequences		
Target	Forward Primer (5'-3')	Reverse Primer (5'-3')
Wild Type	CACCATGAGGCGCGCGCCTTCCC	CTAGTCACGCTGGGCAGCGTAG

*The underlined CACC in the forward primer provides part of the Kozak consensus sequence and allows for directional cloning

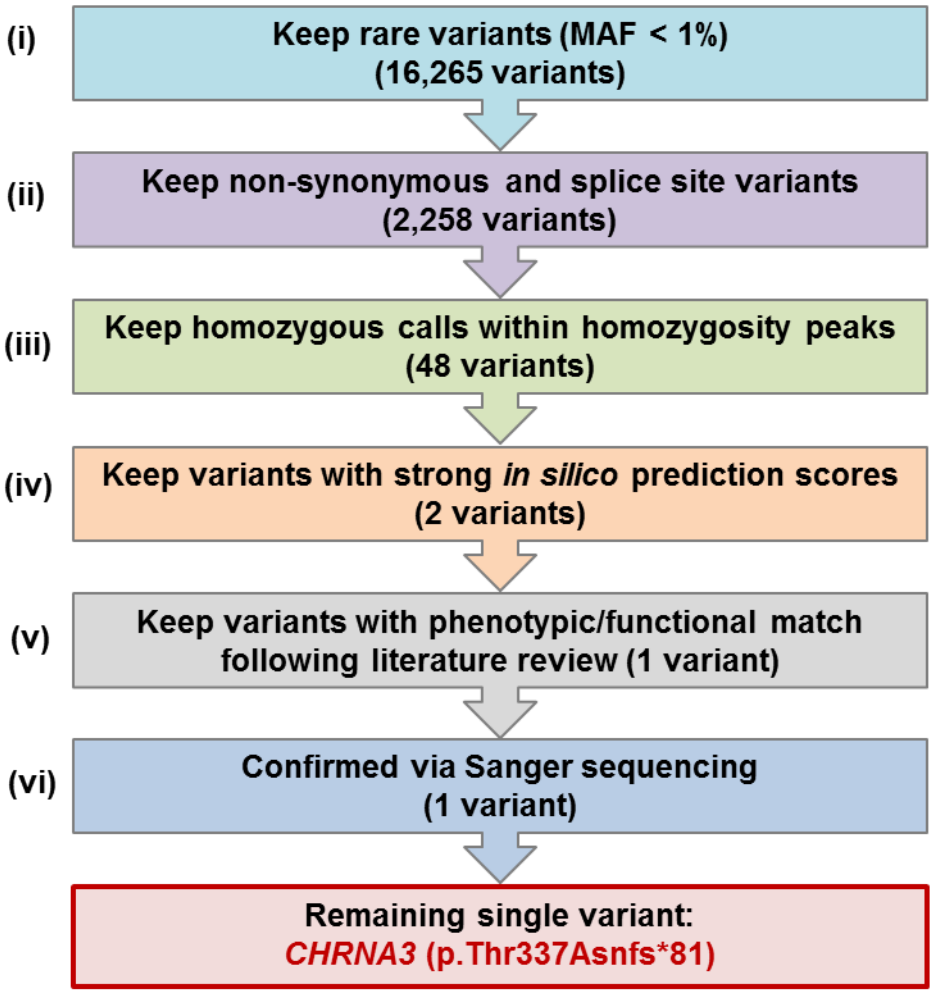

Figure S1. Variant filtering process from whole exome sequencing data for the proband from the index family, B1717-21.

i) Keep rare variants that are present with a minor allele frequency (MAF) <1% in healthy control cohorts (NHLBI Exome Sequencing Project, Exome Aggregation Consortium, Genome Aggregation Database, 1000 Genomes Project).

ii) Keep non-synonymous variants and intronic variants that are located within splice sites.

iii) Due to presence of consanguinity, apply an autosomal recessive hypothesis and overlap surviving variants with the homozygosity mapping. Keep all homozygous calls within the regions of homozygosity by descent.

iv) Rank remaining variants based on their predicted likelihoods of being deleterious for the function of the encoded protein. Keep variants that are protein-truncating (i.e. nonsense, frameshift, obligatory splice, or loss of start or stop codons) or that are highly conserved across phylogeny and predicted to be deleterious based on at least two of three prediction programs (PoyPhen2, SIFT, and MutationTaster).

v) Review literature on remaining variants, and keep variants with known role in the kidney or bladder, or with animal models that match the patient phenotype.

vi) Sanger confirm variant in original DNA.

The only remaining variant following this process was a homozygous truncating mutation in *CHRNA3* (Thr337Asnfs*81).

A Renal and Bladder Imaging for B1402

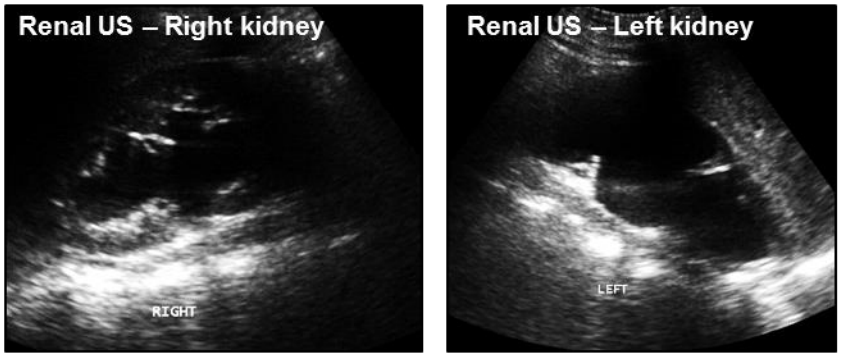

B Renal and Bladder Imaging for B1717-21

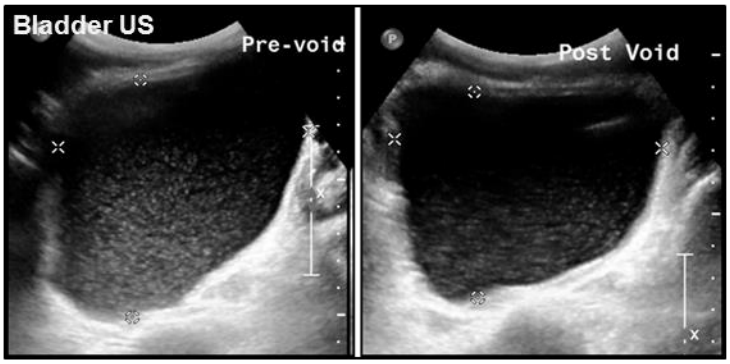

C Renal and Bladder Imaging for GM-21

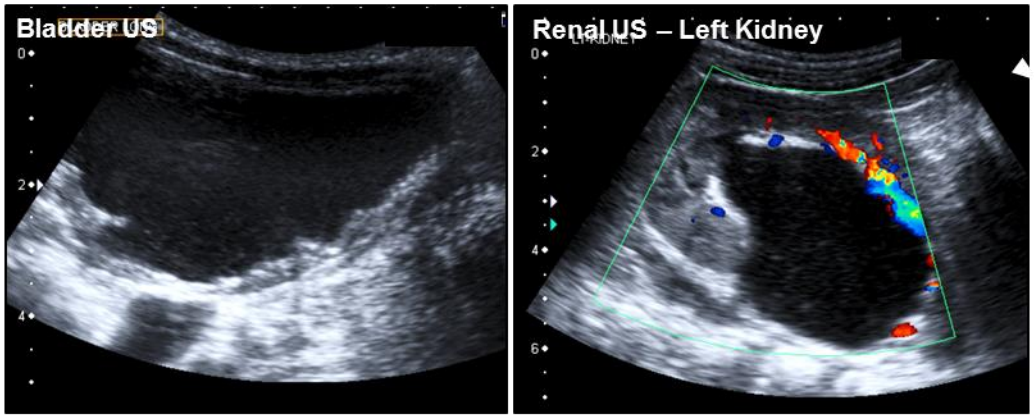

Figure S2. Additional renal and bladder imaging.

(A) Imaging for individual B1402. Renal ultrasounds depicting bilateral hydronephrosis.

(B) Imaging for individual B1717-21. Pre- and post-void ultrasound imaging of the bladder depict poor bladder emptying with a large post-void residual.

(C) Imaging for individual GM-21. Bladder ultrasound (left image) depicts a thickened, trabeculated bladder wall, while renal ultrasound (right image) demonstrates marked hydronephrosis and cortical thinning.

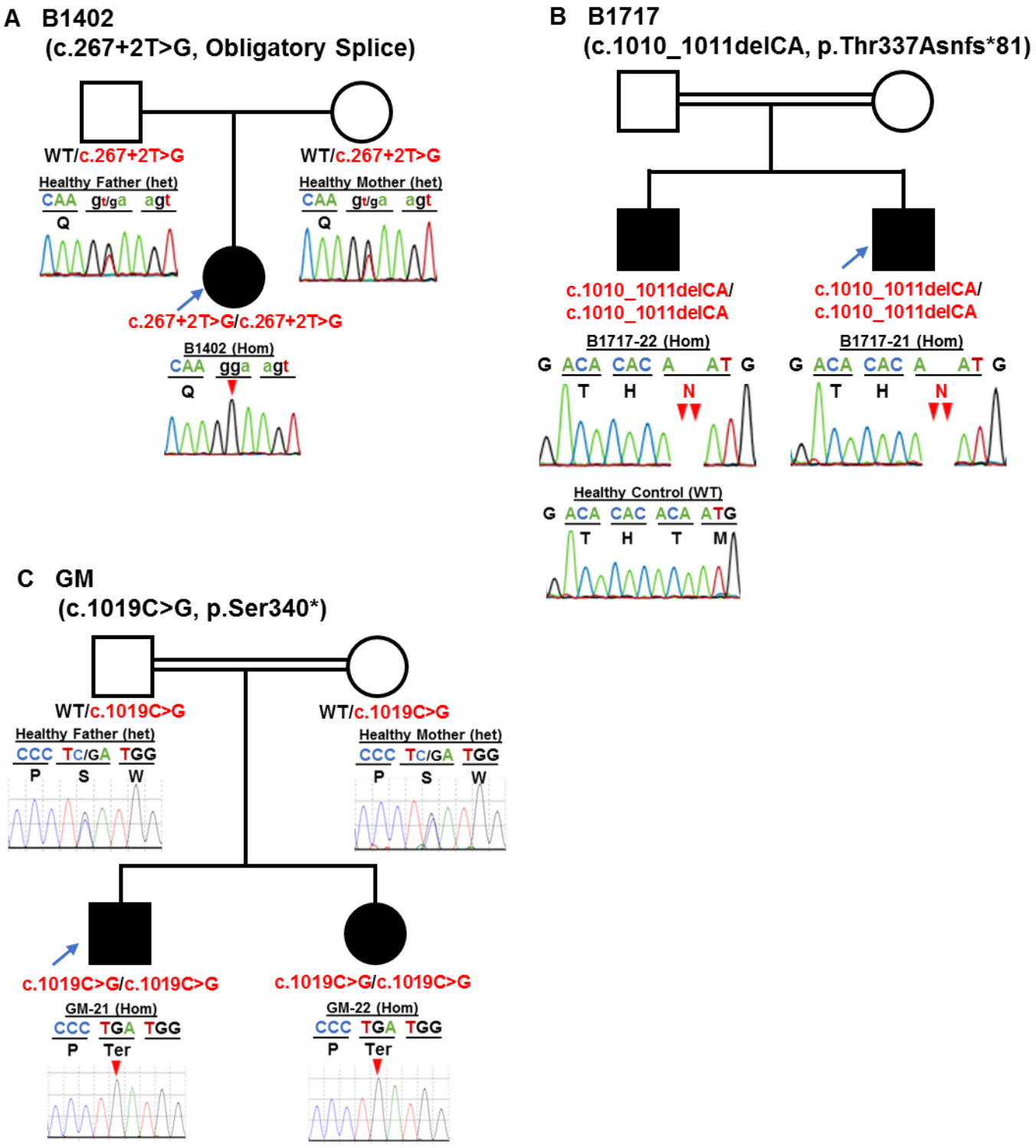

Figure S3. Sanger sequencing for three families with mutations in *CHRNA3*.

The pedigrees and Sanger tracings for the three families (**A-C**) in whom mutations in *CHRNA3* were identified are depicted here. In the pedigrees, squares represent males and circles represent females. Open symbols represent unaffected individuals, and filled symbols represent affected individuals. Consanguineous unions are depicted as double horizontal lines. Individual genotypes from Sanger sequencing are shown. Probands are denoted by blue arrows.

het, heterozygous; Hom, homozygous; Ter, termination; WT, wild type

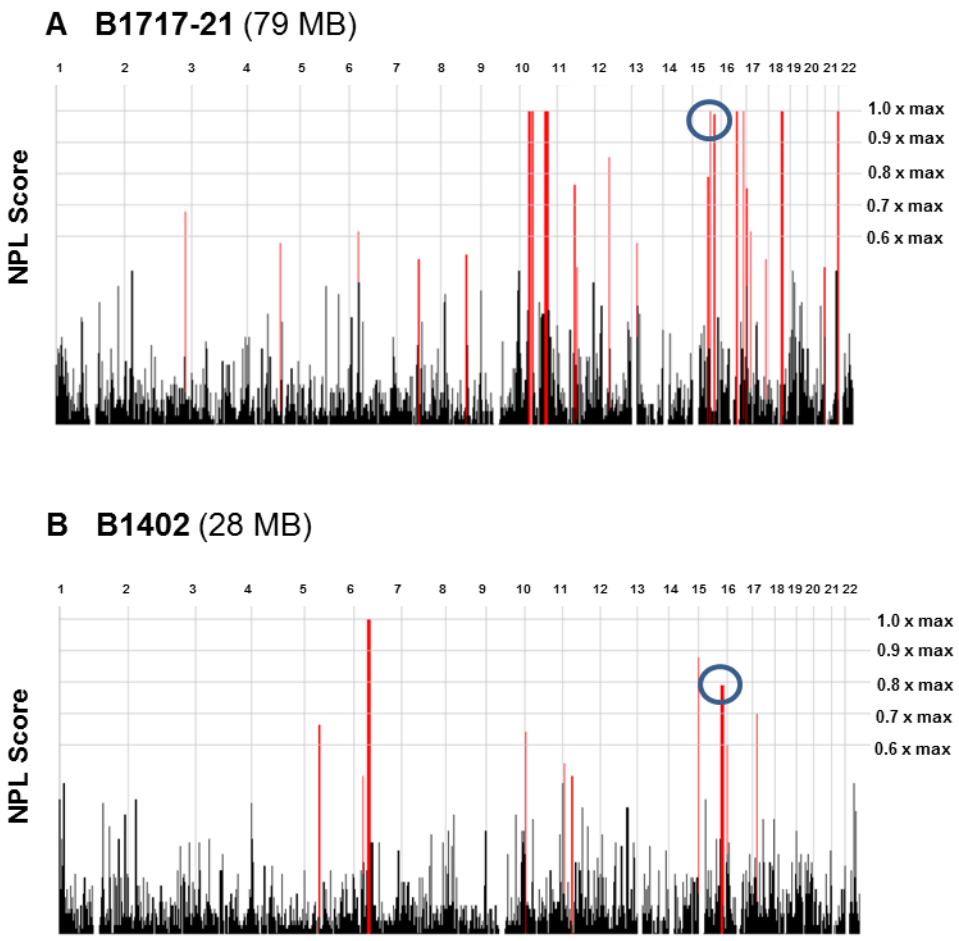

Figure S4. Homozygosity mapping for affected individual B1717-21 and B1402.

Homozygosity mapping for two affected individuals, B1717-21 and B1402, is depicted here. Chromosomal position is aligned along the X-axis. Peaks (red) indicate regions of homozygosity by descent. Both probands have a peak on chromosome 15 where *CHRNA3* is located. The megabases (MB) of homozygosity for each patient is indicated in the figure captions.

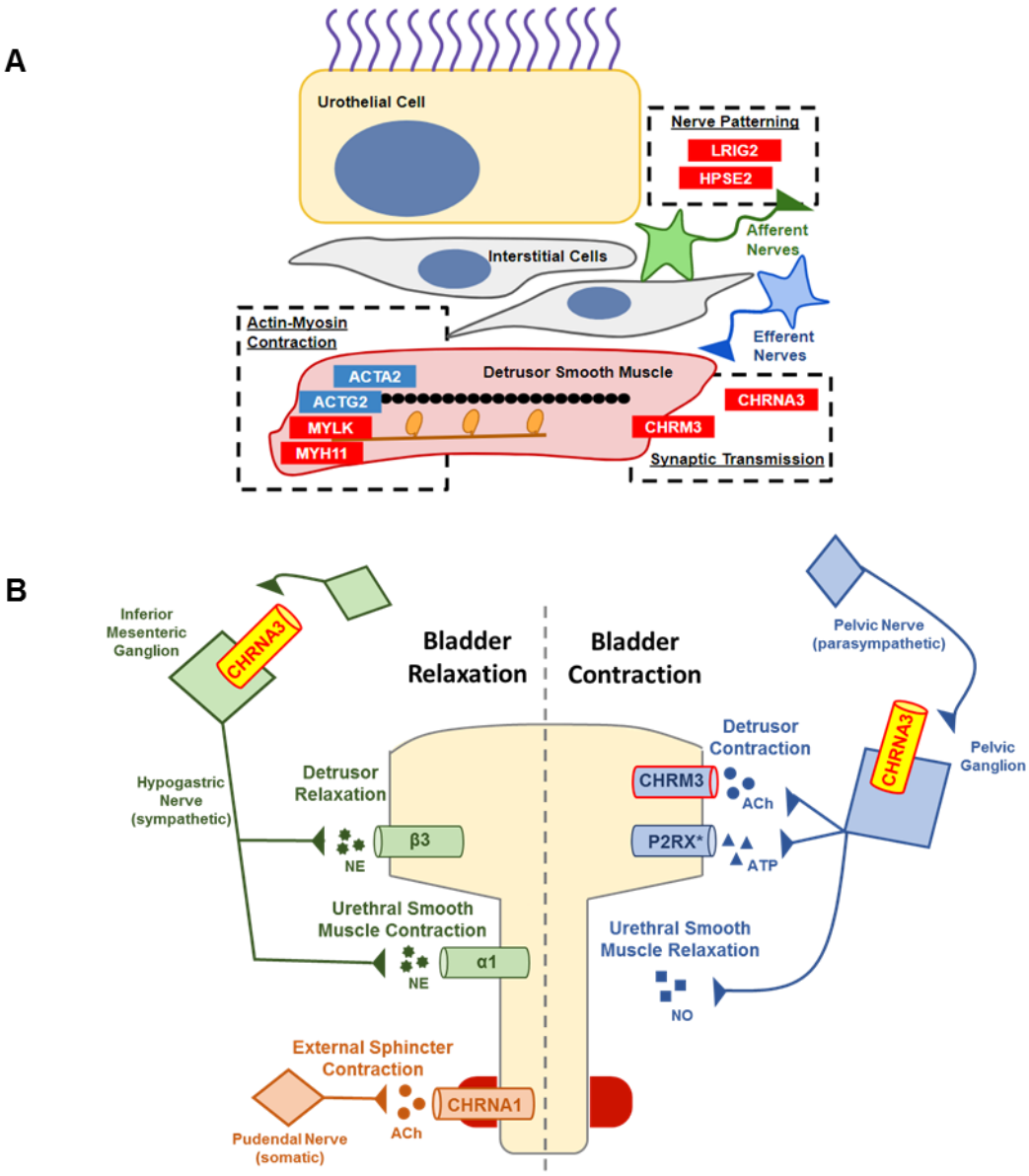

Figure S5. Monogenic causes of bladder dysfunction.

(A) Schematic of monogenic causes of bladder dysfunction. This includes mutations in genes that disrupt actin-myosin contraction of the detrusor smooth muscle *(ACTA2, ACTG2*, *MYLK*, *MYH11*), genes that disrupt neuronal patterning (*LRIG2*, *HPSE2*), as well as genes that affect neuronal synaptic transmission (*CHRNA3*, *CHRM3*). Genes in red are inherited in an autosomal recessive fashion, while those in blue are inherited in an autosomal dominant manner.

(B) Schematic diagram depicting the neuronal innervation to the bladder and the role of *CHRNA3* in regulating bladder and urethral relaxation and contraction. *CHRNA3* is expressed in both the sympathetic (green) and parasympathetic (blue) ganglia. The sympathetic nervous system mediates bladder relaxation. The post-ganglionic hypogastric nerve stimulates β3 and α1 adrenergic receptors to mediate detrusor relaxation and urethral smooth muscle contraction, respectively. The parasympathetic nervous system is activated during voiding, and mediates detrusor contraction via muscarinic acetylcholine receptors (*CHRM3*) and purinergic receptors (*P2RX**). It also mediates urethral smooth muscle relaxation via nitrous oxide signaling. Muscle-type nicotinic acetylcholine receptors also facilitate contraction of the external urethral sphincter (orange). The receptors encoded by genes that, if mutated, cause monogenic forms of CAKUT (*CHRM3*, *CHRNA3*) are outlined in red.

Adapted from Fowler et al., *Nature Reviews Neuroscience*, 9:452, 2008.

REFERENCES

1. Braun DA, Lovric S, Schapiro D, Schneider R, Marquez J, Asif M, Hussain MS, Daga A, Widmeier E, Rao J, et al. Mutations in multiple components of the nuclear pore complex cause nephrotic syndrome. *The Journal of clinical investigation.* 2018;128(10):4313-28.
2. Hildebrandt F, Heeringa SF, Ruschendorf F, Attanasio M, Nurnberg G, Becker C, Seelow D, Huebner N, Chernin G, Vlangos CN, et al. A systematic approach to mapping recessive disease genes in individuals from outbred populations. *PLoS genetics.* 2009;5(1):e1000353.
3. MacArthur DG, Manolio TA, Dimmock DP, Rehm HL, Shendure J, Abecasis GR, Adams DR, Altman RB, Antonarakis SE, Ashley EA, et al. Guidelines for investigating causality of sequence variants in human disease. *Nature.* 2014;508(7497):469-76.
4. Sobreira N, Schiettecatte F, Valle D, and Hamosh A. GeneMatcher: a matching tool for connecting investigators with an interest in the same gene. *Human mutation.* 2015;36(10):928-30.
5. Sobreira N, Schiettecatte F, Boehm C, Valle D, and Hamosh A. New tools for Mendelian disease gene identification: PhenoDB variant analysis module; and GeneMatcher, a web-based tool for linking investigators with an interest in the same gene. *Human mutation.* 2015;36(4):425-31.